4

Antagonistic Actuation Principle for a Silicone-based Soft Manipulator

Ali Shiva[1], Agostino Stilli[1], Yohan Noh[1], Angela Faragasso[1], Iris De Falco[2], Giada Gerboni[2], Matteo Cianchetti[2], Arianna Menciassi[2], Kaspar Althoefer[1], and Helge A. Wurdemann[1]

[1]Department of Informatics, King's College London, London, United Kingdom
[2]The BioRobotics Institute, Scuola Superiore Sant'Anna, Pontedera (PI), Italy

Abstract

This chapter proposes an alternative actuation principle that investigates the capability of variable stiffness of a continuum silicon-based manipulator which was primarily developed for Minimally Invasive Surgery (MIS). Inspired by biological muscular composition, we have designed a hybrid actuation mechanism that can be alternatively used for STIFF-FLOP manipulator. The current soft robot is actuated by pneumatic pressure, in addition to incorporating tendons' tension, which are placed within the soft robot's body. Experiments are conducted by exerting an externally applied force in different poses, and simultaneously varying the stiffness via the tendons. Test results are demonstrated, and it is observed that dual antagonistic actuation, with the benefit of higher force capacities, could indeed promise enhancing soft robotics morphological features.

4.1 Introduction

Researchers have shown increasing interest in robotic systems which could potentially overcome some limitations of conventional robots with rigid joints and links [1]. Looking into biological examples, animals' appendages such as the octopus arm have been the inspiration for developing soft and hyper-redundant robots and aiming to achieve similar capabilities as their biological

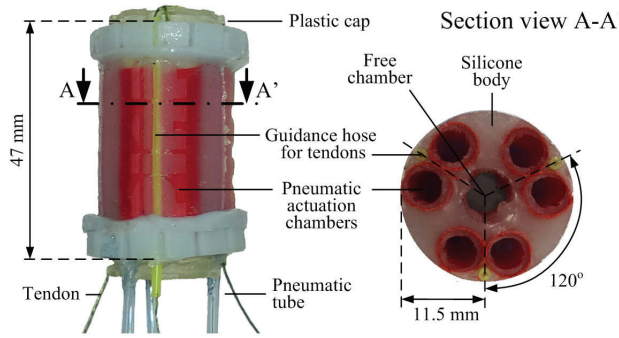

Figure 4.1 Side and cross-section view of a segment/module of the STIFF-FLOP manipulator with integrated stiffening mechanism based on the antagonistic principle: Three pairs of pneumatically actuated chambers are located in a silicone body. Between each set, a hose is integrated into the periphery of the manipulator to guide the tendons that are used to apply stiffening.

counterparts [2–5]. The application of these type of robots can result in significant improvements within a number of fields where traditional robots are currently used [6–8]. One of these areas is Minimally Invasive Surgery (MIS)—also called laparoscopic or keyhole surgery [9, 10]. In minimally invasive procedures, rigid laparoscopic tools are inserted through 12–15 mm incisions called Trocar ports which facilitates surgeries within the body [11]. Multiple challenges have been reported on the limited maneuverability of rigid surgical tools [11, 12] during a number of procedural steps in MIS such as posterior and lateral Total Mesorectal Excision (TME). In this regard, soft robotics has demonstrated immense potential [11]. The soft structure is beneficial due to reducing unwanted abrasion of internal tissue. The large Degrees of Freedom (DoF) shows promising for navigation around internal organs to reach a specific target, rather than cutting and therefore damaging healthy tissue. However, in employing soft robots, there exists a challenge on how to achieve higher stiffness and how to adjust it when dealing with different environments and tissues when we need to apply various forces [13].

A background on stiffness mechanisms is presented in Section 4.2. Section 4.3 gives the details of the dual actuation mechanism. The mechanical design of the soft, stiffness-controllable robot arm is presented in Section 4.4 along with the overall control architecture. Section 4.5 introduces the experimental methodology to investigate the efficiency of the variable stiffness mechanism and demonstrate the results. Finally, conclusions and future works are presented in Section 4.6.

4.2 Background

Recently, researchers have shown interest in finding appropriate methods for the position, force, and stiffness control of soft manipulators. Along these lines, the STIFF-FLOP focuses on studying such mechanisms within the octopus, and attempts to replicate some relevant biological characteristics to develop medical robotics systems for Minimally Invasive Surgery (MIS) [14] with integrated sensors [15–18]. Stiffness control is achieved with an embedded chamber within the silicone body containing granule that can be jammed by applying a vacuum [13, 19–21]. Hence, the manipulator's pose can be made more robust and resilient in a desired position. The concept of polymeric artificial muscles described in [22] to actuate a robot manipulator was furthered in [23] by integrating granule-filled chambers which when exposed to varying degrees of vacuum could actuate, soften, and stiffen the manipulator's joints. A similar concept is proposed in [24]. A hollow snake-like manipulator consists of multiple overlapping layers of thin Mylar film. By applying vacuum pressure, the friction between the film layers increases, which results in a tunable stiffness capability. In [25], the authors report on a thermally tunable composite for mechanical structures. This flexible open-cell foam coated in wax can change stiffness, strength, and volume. Altering between a stiff and soft state and vice versa introduces a time delay as the material does not instantly react to the heating-up or cooling-down process.

Here, the hybrid actuation principle has been applied to the STIFF-FLOP manipulator. Air pressure is mainly used for stretching out and controlling the motion and direction of the soft manipulator. When stiffness increase is required, tendons are manipulated in such a way as to oppose the pneumatic actuation. The results show the capabilities of adopting this antagonistic actuation scheme and the main advantages of the proposed technique when compared to traditional, single-actuation-type robot manipulators and to stiffening mechanism such as granular jamming.

4.3 Bio-Inspiration and Contributions

The work presented here has been inspired by the soft tentacles of octopi that demonstrate infinite DoFs. The tentacle comprises longitudinal and transverse muscles, bonded within the arm. Figure 4.2 gives an overview of the arm's structure. Different muscles are manipulated in such a way as to control the stiffness of its arm according to the nature of the task at hand.

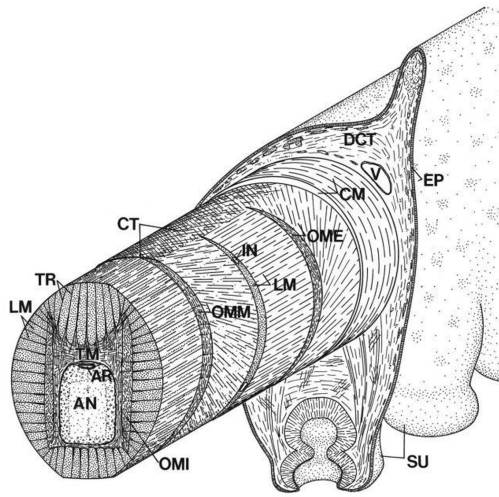

Figure 4.2 Three-dimensional illustration of an octopus tentacle with showing longitudinal muscle fibres (LM), transverse muscle fibres (TM) and connective tissue (CT). These types of muscles are primarily used by the octopus to create a range of stiffness along its arms [26].

Hence, by keeping the principles of operation of the biological counterpart in mind, our proposed manipulator utilizes the two actuation mechanisms: fluidic, and tendon-based, with the ability to oppose each other and thus capable of varying the arms' stiffness over a wide range. Hence, the proposed antagonistic actuation method bring together the advantages of fluidic and tendon-driven actuation. Tendon-based actuation is desirable when more precise position control is needed, and/or higher external forces are to be experienced. Stepper motors that are used to extend/flex each tendon are externally based [27, 28]. Pneumatic actuation is suitable for inherently safe scenarios such as handling delicate tasks where softness is required, in addition to generating a wider range of motion.

4.4 Integration of the Antagonistic Stiffening Mechanism

One segment/module of the STIFF-FLOP manipulator (see Figure 4.3) is a hollow cylinder of silicone made of Ecoflex® $00-50$ Supersoft Silicone with material properties as shown in Table 4.1. The segment has an overall length of $47\,\mathrm{mm}$ and an outer diameter of $23\,\mathrm{mm}$. In the periphery of this cylinder, three pairs of reinforced fluidic pressure chambers ($6\,\mathrm{mm}$ diameter) are

Table 4.1 Technical properties of Ecoflex® 00 − 50 Supersoft Silicone[1]

Shore Hardness	Tensile Strength	Elongation at Break
00 − 50	315 psi	980%

implemented which are actuated pneumatically. Each dual fluidic chamber is connected to one 2 mm outer diameter inlet air pipe creating the ability to bend the module by increasing the air pressure in one dual chamber relative to the other two fluidic chambers. Simultaneous pressurization of the all dual chambers results in overall elongation of the segment. For the sake of completeness, the segment's structure in Figure 4.3 shows an inner free chamber of 9 mm diameter. This space is generated to pass through tubes from additional segments and wires from integrated sensory systems when creating a manipulator with a series of multiple modules.

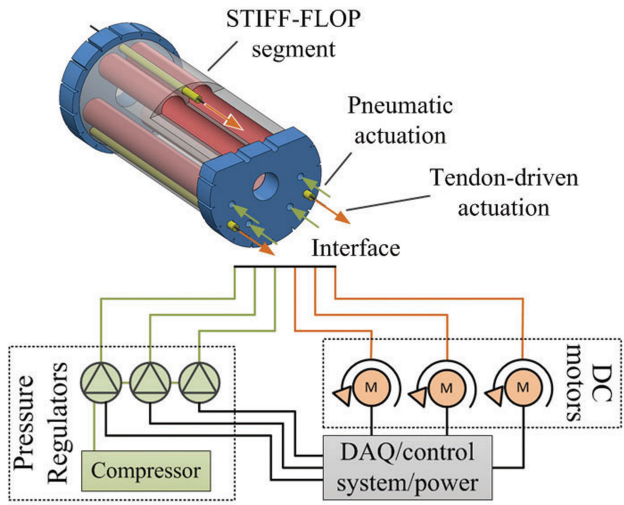

Figure 4.3 Schematic overview of the antagonistic actuation setup: The air chambers are connected to three pressure regulators. An air compressor supplies pressurised air to the regulators. Each tendon is wound around a pulley which is fixed to the shaft of a stepper motor. The analogue input for the three motors and three pressure regulator is controlled via a data acquisition board.

[1] Smooth-On, Inc. *Ecoflex® Series* Available on http://www.smooth-on.com/tb/files/ECOFLEX_SERIES_TB.pdf, Accessed on May 2015.

4.4.1 Embedding Tendon-driven Actuation into a STIFF-FLOP Segment

The tendon-driven actuation mechanism is embedded into a single STIFF-FLOP segment. Figure 4.3 shows a side and cross-sectional view of the robot arm with the integrated antagonistic actuation principle. In this prototype, a hose (made of stretchable latex tubes with a diameter of $1.6\,\mathrm{mm}$) is aligned in between each set of the fluidic chambers, hence being parallel to the longitudinal axis. The three hoses are placed 120° from each other feeding through tendons for extrinsic actuation. This design will allow the tendons to slide within the latex tubes and avoid any cuts into the silicone body. Due to the tube's material properties, the STIFF-FLOP segment keeps its key characteristics of being soft and squeezable; the latex tubes move in a compliant way when intrinsically actuating the robot.

Through each of the three passages, we pass a microfilament-braided PowerPro Super Line of $0.15\,\mathrm{mm}$ diameter acting as tendons. The three tendons are fixed to a plastic cap at the tip of the robot arm to distribute forces onto the soft tip surface when applying tension. The entire combination of the aforementioned configuration constructs one segment, which is shown in Figure 4.3.

4.4.2 Setup of the Antagonistic Actuation Architecture

The overall actuation architecture consists of an air compressor, three pressure regulators, a data acquisition board (DAQ), three stepper motors, and a modified STIFF-FLOP segment as described in Section 4.4.1. Figure 4.3 presents the interconnection within the test setup.

As mentioned earlier, a hybrid actuation mechanism is employed here: On the pneumatic actuation side, an air compressor (BAMBI MD Range Model 150/500) supplies the required pressurised air of $5\,\mathrm{bar}$ to three independent pressure regulators (SMC ITV0030-3BS-Q). The output three dual fluidic chambers of the soft module via with 0 to $10\,\mathrm{VDC}$ input signal and a set pressure range of 0.001 to $0.5\,\mathrm{MPa}$. Each pressure regulator adjusts the outlet pressure for each dual fluidic chamber according to the command received from the computer through a DAQ board (NI USB-6411).

On the tendon side, each tendon is connected to a stepper motor (Changzhou Songyang Machinery & Electronics Co. SY57ST56-0606B) which provides a holding torque of $0.59\,\mathrm{Nm}$. Each stepper motor has a pulley attached on the output shaft which the tendon is wound around. The pulley has $6.4\,\mathrm{mm}$ radius, which results in a maximum of $92.6\,\mathrm{N}$ of tension.

Since one STIFF-FLOP segment has three tendons, three stepper motors are taken into consideration. Each stepper motor is driven via a driver (Big Easy Driver ROB-11876), which communicates with the computer via a DAQ board. The computer has a Windows-based operating system with the related programming in C++.

4.5 Test Protocol, Experimental Results, and Discussion

4.5.1 Methodology

Various experiments for stiffness characterization have been carried out by hanging the manipulator and exerting external force at the distal end. A command for the computer generates a displacement of $1\,\mathrm{cm}$ for the linear rail mechanism which presses against the tip of the module. Reaction forces are recorded utilizing a Nano17 Force/Torque sensor by ATI Industrial Automation. The experimental configurations were defined as follows:

Scenario 1:
The module is held vertically downwards. The force is applied laterally to the tip as shown in Figure 4.4(a). In this scenario, four different sub-cases are investigated:

- **A** No air pressure and no tendon tension.
- **B** Equally air-pressurised chambers (i.e. elongation) with no tendon tension.
- **C** No air pressure with initial equal tendon tension.
- **D** Equally air-pressurised chambers with initial equal tension in tendons.

Scenario 2:
The module is held vertically and one of the dual chambers is pressurised to form a 90% curved shape, and the force is applied laterally as shown in Figure 4.4(b). Two different sub-cases are investigated:

- **A** One pressurized chamber and no tendon tension.
- **B** One pressurized chamber and tension in the tendons.

Scenario 3:
The module is pressurized to be configured as Scenario 2. However, the force is applied opposing the tip as shown in Figure 4.4(c). Also in this scenario, two different sub-cases are investigated:

- **A** One pressurised chamber and no tendon tension.
- **B** One pressurized chamber and tension in the tendons.

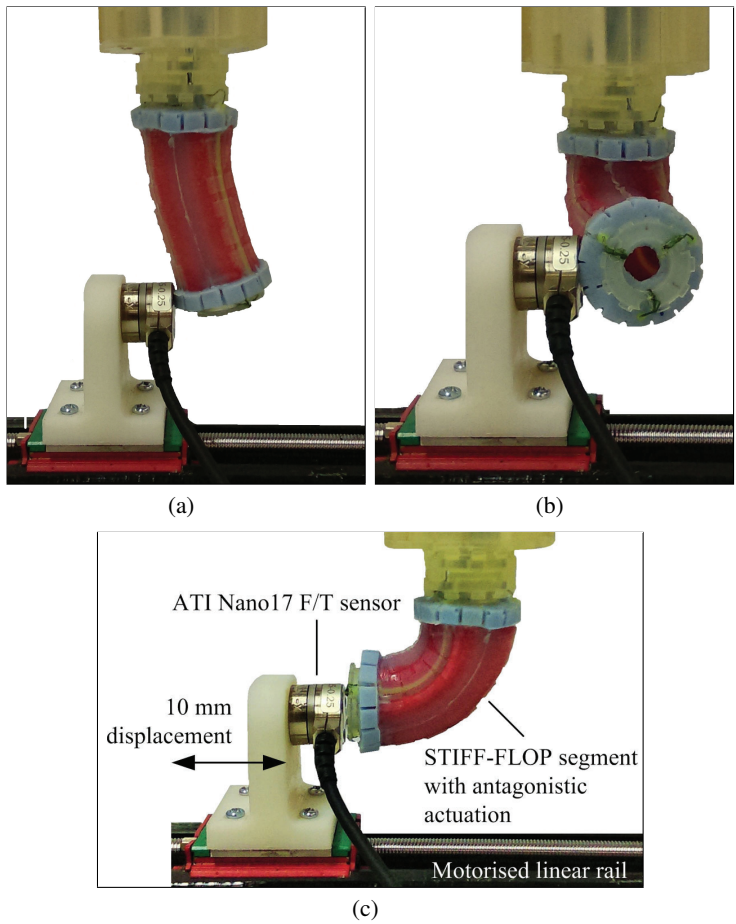

Figure 4.4 An ATI Nano17 Force/Torque sensor is mounted on a motorised linear mechanism displacing the manipulator's tip by 1 cm: The configurations in (a), (b), and (c) show Scenarios 1, 2, and 3, respectively.

4.5.2 Experimental Results

Data from the ATI Nano17 F/T sensor and corresponding displacement of the motorized linear module were recorded at 1 kHz using a DAQ card (NI USB-6211). Four trials were performed for each sub-case.

Experimental results of all four sub-cases of Scenario 1 are presented in Figure 4.5(a). When the module is neither pressurized nor stiffened by tendons, the amount of its resistive force subjected to a 1 cm lateral displacement

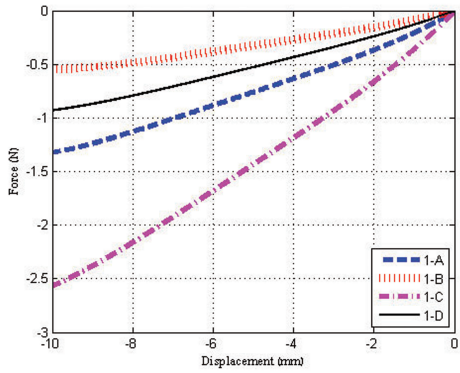

(a)

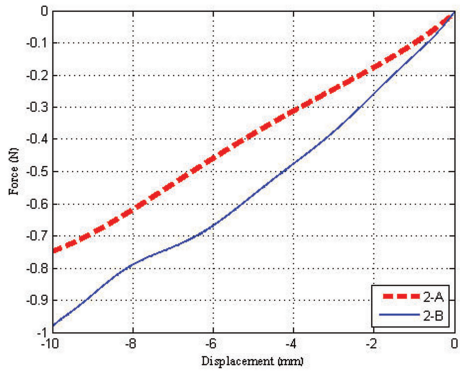

(b)

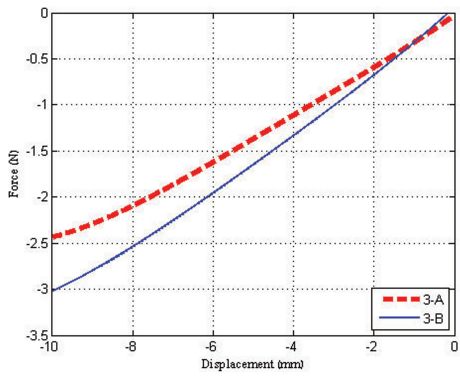

(c)

Figure 4.5 Experimental data for Scenarios 1, 2, and 3. Forces have been recorded for displacements of 1 cm of the manipulator's tip. Table 4.2 summarises the data analysis.

is about $1.32\,\mathrm{N}$. This value is $0.55\,\mathrm{N}$ when all three chambers are pressurized. When subjected to tendon stiffening, the resistive forces displayed by the module reach to $2.56\,\mathrm{N}$ and $0.93\,\mathrm{N}$, respectively, showing a 94% and 69% increase compared to the first and second sub-case.

The results of the two sub-cases of Scenario 2 are shown in Figure 4.5(b). When the module is only pressurised, the value of the resistive force is $0.75\,\mathrm{N}$. With tendon stiffening is added to the module, this resistive force increases to $0.98\,\mathrm{N}$ showing a 31% growth.

The results of the two sub-cases for Scenario 3 are presented in Figure 4.5(c). It can be seen that in the presence of pressure only, the module generates a resistive force of $2.43\,\mathrm{N}$. However, by introducing tendon stiffening, the resistive force due to $1\,\mathrm{cm}$ displacement intensifies to $3.02\,\mathrm{N}$, displaying a 24% growth.

Table 4.2 summarizes the experimental results. For each sub-case, the maximum force, hysteresis, and percentage of increase is calculated.

4.5.3 Discussion

Experimental results in Table 4.2 and Figure 4.4 demonstrate that incorporating the dual actuation mechanism has improved the stiffness of the STIFF-FLOP module up to almost 100%. In this sense, we are able to deal with higher external forces, and/or resist external disturbances more effectively during task execution. This gives the surgeon the ability to move the manipulator about primarily with pressure actuation, and thereafter, use the tendon stiffening to acquire not only higher stiffness values, but also fine-tune the final position of the end effector for more accurate maneuvering.

Table 4.2 Summarized results of stiffness tests for Scenarios 1, 2, & 3

Scenarios					F_{max}	Hyst.	Increase
1-A	Tens.	No	Press.	No	1.32 N	21.6%	n/a
1-B	Tens.	No	Press.	Yes	0.55 N	27.2%	n/a
1-C	Tens.	Yes	Press.	No	2.56 N	18.9%	93.9%
1-D	Tens.	Yes	Press.	Yes	0.93 N	28.5%	69.1%
2-A	Tens.	No	Press.	Yes	0.75 N	21.8%	n/a
2-B	Tens.	Yes	Press.	Yes	0.98 N	33.46%	30.7%
3-A	Tens.	No	Press.	Yes	2.43 N	27.47%	n/a
3-B	Tens.	Yes	Press.	Yes	3.02 N	14.86%	24.3%

Table 4.3 Force results for granular jamming applying a 10 mm displacement as reported in [9]

Scenarios	Granular Jamming	F_{max}	Increase
1-A	Off	2.2 N	n/a
1-A	On	3.1 N	40.9%
2-A	Off	2.3 N	n/a
2-A	On	2.7 N	17.4%
3-A	Off	2.8 N	n/a
3-A	On	3.3 N	17.9%

In [9], an 8 mm diameter channel of granular material, coffee, was embedded into a previous version of the silicone-based STIFF-FLOP module. The length of this segment was 50 mm with the silicone structure having a diameter of 25 mm. The pneumatically actuated chambers were not reinforced; a crimped, braided sheath of 35 mm covered the silicone structure and prevented a ballooning effect. Neglecting the outer cover, the STIFF-FLOP module has similar dimensions as the segment used in this chapter. The key experimental results for stiffness tests at a displacement of 10 mm are summarized in Table 4.3. The test configurations of three scenarios are equivalent to the ones described in Section 4.5.1; however, stiffening is activated by applying a vacuum of 36%.

Comparing Tables 4.2 and 4.3, the actual maximum forces F_{max} measured during the experimental tests of Scenarios 1 and 2 are larger using granular jamming. The presence of coffee granules (under atmospheric or vacuum pressure) integrated into the silicone-based robot results in a stiffer module. Looking at the percentage increase caused by granular jamming on the one hand and the antagonistic mechanism on the other hand, the bio-inspired tendon-based stiffening principle is able to generate a larger growth. Additionally, adding the tendons has not only resulted in the ability to vary the stiffness, but also acts beneficially towards the position control of the soft manipulator allowing simultaneous position and stiffness control.

4.6 Conclusions

In this chapter, we have proposed the dual actuation mechanism to a soft continuum robot, which enables antagonistic stiffening. This approach can be used as an alternative to the actuation method proposed in Chapter 3. Hereby, air pressure is employed for a wider range of movement such as

elongation and bending, while the tendon-driven system provides the fine-tuned movements in addition to the ability of varying the stiffness. Due to the internal accommodation of the tendons in the wall of the module, this added feature does not increase the overall diameter nor the wall thickness of this soft continuum robot.

Future work is to incorporate a system which would allow adjustment of tendon tensions in a more ergonomic manner.

4.7 Funding

The work described in this chapter is partially funded by the Seventh Framework Programme of the European Commission under grant agreement 287728 in the framework of EU project STIFF-FLOP.

References

[1] Ataollahi, A., Karim, R., Fallah, A. S., Rhode, K., Razavi, R., Seneviratne, L. T., et al. (2013). 3-DOF MR-compatible multi-segment cardiac catheter steering mechanism. *IEEE Trans. Biomed. Eng.* 99:1.

[2] Buckingham, R. (2002). Snake arm robots. *Ind. Robot* 29, 242–245.

[3] Caldwell, D. G., Medrano-Cerda, G. A., and Goodwin, M. (1995). "Control of pneumatic muscle actuators," in *Proceedings of the IEEE Control Systems*, San Diego, CA, 15.

[4] Cheng, N. G., Gopinath, A., Wang, L., Iagnemma, K., and Hosoi, A. E. (2014). Thermally tunable, self-healing composites for soft robotic applications. *Macromol. Mater. Eng.* 299, 1279–1284.

[5] Cianchetti, M., Arienti, A., Follador, M., Mazzolai, B., Dario, P., and Laschi, C. (2011). Design concept and validation of a robotic arm inspired by the octopus. *Mater. Sci. Eng. C* 31, 1230–1239.

[6] Cianchetti, M., Ranzani, T., Gerboni, G., de Falco, I., Laschi, C., and Menciassi, A. (2013). "STIFF-FLOP surgical manipulator: mechanical design and experimental charaterization of the single module," in *Proceedings of the IEEE/RSJ International Conference on Intelligent Robots and Systems*, Hamburg.

[7] Cianchetti, M., Ranzani, T., Gerboni, G., Nanayakkara, T., Althoefer, K., Dasgupta, P., et al. (2014). Soft robotics technologies to address shortcomings in today's minimally invasive surgery: The STIFF-FLOP approach. *Soft Robotics* 1, 122–131.

[8] Cieslak, R., and Morecki, A. (1999). Elephant trunk type elastic manipulator—a tool for bulk and liquid type materials transportation. *Robotica* 17, 11–16.

[9] Fras, J., Czarnowski, J., Macias, M., Glowka, J., Cianchetti, M., and Menciassi, A. (2015). "New STIFF-FLOP module construction idea for improved actuation and sensing," in *Proceedings of the ICRA*, New Orleans, LA.

[10] Godage, I. S., Nanayakkara, T., and Caldwell, D. G. (2012). "Locomotion with continuum limbs," in *Proceedings of the IEEE/RSJ International Conference on Intelligent Robots and Systems*, Deajeon.

[11] Gravagne, I., Rahn, C., and Walker, I. D. (2003). Large deflection dynamics and control for planar continuum robots. *IEEE/ASME Trans. Mech.* 8, 299–307.

[12] Jiang, A., Aste, T., Dasgupta, P., Althoefer, K., and Nanayakkara, T. (2013). "Granular jamming with hydraulc control," in *Proceedings of the ASME International Design Engineering Technical Conferences and Computers and Information in Engineering Conference*, New York, NY.

[13] Jiang, A., Secco, E. L., Wurdemann, H., Nanayakkara, T., Dasgupta, P., and Athoefer, K. (2013). "Stiffness-controllable octopus-like robot arm for minimally invasive surgery," in *Proceedings of the 3rd Joint Workshop on New Technologies for Computer/Robot Assisted Surgery*, Pisa.

[14] Jiang, A., Secco, E., Wurdemann, H. A., Nanayakkara, T., Dasgupta, P., and Athoefer. K. (2013). "Stiffness-controllable octopus-like robot arm for minimally invasive surgery," in *Proceedings of the Workshop on New Technologies for Computer/Robot Assisted Surgery*, Pisa.

[15] Jiang, A., Xynogalas, G., Dasgupta, P., Althoefer, K. and Nanayakkara, T. (2012). "Design of a variable stiffness flexible manipulator with composite granular jamming and membrane coupling," in Proceedings of the *IEEE/RSJ International Conference on Intelligent Robots and Systems*, Vancouver.

[16] Kier, M. W., and Stella, M. P. (2007). The arrangement and function of octopus arm musculature and connective tissue. *J. Morphol.* 268, 831–843.

[17] Kim, Y. J., Cheng, S., Kim, S., and Iagnemma, K. (2012). "Design of a tubular snake-like manipulator with stiffening capability by layer jamming," in *Proceedings of the IEEE/RSJ International Conference on Intelligent Robots and Systems*, Deajeon.

[18] Laschi, C., Mazzolai, B., Mattoli, V., Cianchetti, M., and Dario, P. (2009). Design of a biomimetic robotic octopus arm. *Bio. Biomimetics* 4, 1–8.

[19] Li, M., Ranzani, T., Sareh, S., Seneviratne, L. D., Dasgupta, P., Wurdemann, H. A., and Althoefer, K. (2014). Multi-fingered haptic palpation utilising granular jamming stiffness feedback actuators. *Smart Mater. Struct.* 23:095007.

[20] McMahan, W., Jones, B. A., and Walker, I. D. (2005). "Design and implementation of a multi-section continuum robot: Air-octor," in *Proceedings of the IEEE/RJS International Conference on Intelligent Robots and Systems*, Deajeon.

[21] Neppalli, S., Jones, B., McMahan, W., Chitrakaran, V., Walker, I., Pritts, M., et al. (2007). "Octarm—a soft robotic manipulator," in *Proceedings of the IROS*, Hamburg.

[22] Noh, Y., Sareh, S., Back, J., Wurdemann, H. A., Ranzani, T., Secco, E. L., et al. (2014). "A three-axial body force sensor for flexible manipulators," in *IEEE International Conference on Robotics and Automation*, Montreal.

[23] Noh, Y., Secco, E. L., Sareh, S., Wurdemann, H. A., Faragasso, A., Back, J., et al. (2014). "A continuum body force sensor designed for flexible surgical robotic devices," in *IEEE Engineering in Medicine and Biology Society*, Stockholm.

[24] Ranzani, T., Gerboni, G., Cianchetti, M., and Menciassi, A. (2015). A bioinspired soft manipulator for minimally invasive surgery. *Bio. Biomimet.* 10:035008.

[25] Sareh, S., Jiang, A., Faragasso, A., Noh, Y., Nanayakkara, T., Dasgupta, P., et al. (2014). "Bio-inspired tactile sensor sleeve for surgical soft manipulators," in *Proceedings of the ICRA*, Stockholm.

[26] Walker, I. D., Dawson, D. M., Flash, T., Grasso, F. W., Hanlon, R. T., Hochner, B., et al. (2005). "Continuum robot arms inspired by cephalopods," in *Proceedings of the UGVT VII*, Orlando, FL.

[27] Xie, H., Jiang, A., Wurdemann, H. A., Liu, H. Seneviratne, L. D. and Althoefer, K. (2014). Magnetic resonance-compatible tactile force sensor using fibre optics and vision sensor. *IEEE Sensors J.* 14, 829–838.

[28] Yamashita, H., Iimura, A., Aoki, E., Suzuki, T., Nakazawa, T., Kobayashi, E., et al. (2005). "Development of endoscopic forceps manipulator using multi-slider linkage mechanisms," in *Proceedings of the 1st Asian Symposium on Computer Aided Surgery—Robotic and Image guided Surgery*, Ibaraki.